Myocardial Infarction Induces Sympathetic Nervous Remodeling in Intermediolateral Nucleus

Myocardial Infarction induces Sympathetic Nervous Remodeling in Intermediolateral Nucleus

Minoru Nodera, MD

Department of Cardiovascular Medicine, Fukushima Medical University

論　文　内　容　要　旨

学位論文題名	心筋梗塞後の脊髄中間外側核における交感神経リモデリング現象についての検討

（背景）心筋梗塞後の交感神経活性亢進には星状神経節（SG）の”neural remodeling”という形態学的変化を伴う神経活動亢進が関与していると考えられている。この現象が交感神経系においてSGのみならず他の部位でも認められるのかは明らかにはされていない。

（方法）生後 10～13 週齢の雄ラットの左冠動脈前下行枝を結紮し、心筋梗塞モデルを作成した。その１週間後、あるいは２週間後に脊髄中間外側核(IML: intermediolateral nucleus)が局在する Th2 レベルの胸髄と SG を摘出した。SG 及び IML の neural remodeling については免疫組織染色で評価を行なった。また、リアルタイム PCR 法や蛍光免疫染色により brain-derived neurotrophic factor (BDNF)、tropomyosin-related kinase receptor B (TrkB)の mRNA 及びタンパク発現の検討を行なった。

（結果）心筋梗塞２週間後の SG は Sham 群と比較して神経細胞体の大きさの有意な増加が認められた。同様に IML においても心筋梗塞群で神経細胞体の大きさ及び軸索密度の有意な増加が認められた。次に心筋梗塞１週間後の胸髄における神経成長因子の一つ BDNF およびその受容体 TrkB の mRNA の発現は、sham 群に比して有意に増加していた。免疫蛍光染色による検討によっても、IML における BDNF および TrkB のタンパク発現が心筋梗塞群において有意に増加していることが示された。最後に IML における BDNF-TrkB の発現の増加に伴い、細胞内の成長シグナルが亢進しているか否かを確認するために、ERK（Extracellular signal-regulated kinase）の活性を免疫蛍光染色により検討した。リン酸化 ERK、すなわち活性化 ERK 陽性細胞の割合は心筋梗塞群において有意に高値であった。

（考察）心筋梗塞後の IML の neural remodeling を神経細胞体の腫大と軸索増生により初めて明らかにした。SG のみならず IML も neural remodeling をきたすことから、心筋梗塞後には交感神経系全体において neural remodeling が生じることにより活性の亢進が持続する可能性がある。IML において BDNF 及び TrkB の発現増加及び ERK 活性の亢進が認められたことから、IML の neural remodeling は BDNF/TrkB 経路を介する現象と推察される。胸髄における BDNF の mRNA の発現増加については、その局在は明らかではないが、BDNF の mRNA は IML の位置する脊髄中間層にのみ局在することを考慮すると、IML で増加していた BDNF の由来は IML の細胞体による autocrine、あるいはグリア細胞からの paracrine の可能性が考えられる。

（結論）心筋梗塞後においては SG のみならず IML も neural remodeling をきたす。IML の neural remodeling には BDNF/TrkB 経路の活性化が関与していることが示唆される。

Abstract

Background: Several studies have shown that neural remodeling in stellate ganglia (SG) is induced by myocardial infarction (MI). It remains unclear whether neural remodeling after MI is limited in SG within the sympathetic nervous system.

Methods: MI was induced in a rat model by ligation of the left anterior descending artery. Neural remodeling in the intermediolateral nucleus (IML) and SG was assessed by immunohistochemistry 2 weeks after MI. The mRNA and protein expressions of brain-derived neurotrophic factor (BDNF), tropomyosin-related kinase receptor (TrkB) and extracellular signal-regulated kinase (ERK) were measured by quantitative RT-PCR, immunohistochemistry and Western blotting 1 week after MI.

Results: The neuronal size and axonal density of IML were increased after MI compared to sham (193.5±16.0 vs. 169.1±8.5 μm^2, $P<0.01$; 60587±21767 vs. 31380±17026 $\mu m^2/mm^2$, $P<0.05$, respectively). The density of growth-associated protein-43, a protein upregulated in axons undergoing nerve sprouting, was increased after MI compared to sham. The fluorescence intensity of BDNF and TrkB in IML were significantly higher in the MI group than in the sham group (54750±20047 vs. 28668±12717 $\mu m^2/mm^2$, $P<0.05$). In addition, mRNA expression of BDNF and TrkB in the spinal cord at the Th2 level was increased after MI (1.8±0.9-fold change vs. sham, $P<0.01$; 1.3±0.2-fold change vs. sham, $P<0.05$, respectively). Finally, the percentage of

phospho-ERK-immunoreactive neurons in IML was significantly higher in the MI group than in the sham group.

Conclusions: Neuronal remodeling in IML as well as in SG is induced after MI probably via activation of the BDNF-TrkB axis. Morphological remodeling throughout the sympathetic nervous system may be involved in sustained activation of sympathetic tone after MI.

Keywords: neural remodeling, myocardial infarction, sympathetic nervous system, stellate ganglion, intermediolateral nucleus, brain-derived neurotrophic factor, tropomyosin-related kinase receptor B

Abbreviation

BDNF	brain-derived neurotrophic factor
ChAT	choline acetyltransferase
GAP43	growth-associated protein-43
IML	intermediolateral nucleus
MI	myocardial infarction
NGF	nerve growth factor
pERK	phospho-extracellular signal-regulated kinase
SG	stellate ganglion
SNS	sympathetic nervous system
TH	tyrosine hydroxylase
Trk	tropomyosin-related kinase receptor

Introduction

Recent studies have shown that myocardial infarction (MI) induces neural remodeling in stellate ganglion (SG) (2, 15, 20, 21, 26, 39), where most postganglionic sympathetic neurons that project to the heart exist (24, 25). Neural remodeling is accompanied by morphological remodeling in the form of cellular hypertrophy and nerve sprouting. Neural remodeling occurs as a result of a regenerative process of disrupted sympathetic innervation in the infarct area to recover control of cardiac performance, but heterogeneous reinnervation triggers abnormal sympathetic excitement that is associated with the development of fatal ventricular tachyarrhythmia and sudden cardiac death (3, 9, 10, 29, 40). It is possible that neural remodeling of the whole SNS may cause further sympathetic excitement, and if so, elucidation of pathophysiological mechanisms of neural remodeling throughout the SNS may lead to a novel therapeutic approach for suppressing abnormal sympathetic excitement after MI. The intermediolateral nucleus (IML), where preganglionic sympathetic neurons exist, is located upstream of SG in the SNS. IML exists between dorsal and ventral horns at a lateral position in gray matter of the thoracic spinal cord. The sympathetic nerve in IML expresses tropomyosin-related kinase receptor B (TrkB), which is a receptor of brain-derived neurotrophic factor (BDNF) (5, 18, 30). In the present study, we examined whether MI induced neuronal

remodeling of IML, and if so, investigated the underlying mechanism, with special focus on the BDNF-TrkB axis.

Methods

Ethical statements

We conformed to the Guide for the Care and Use of Laboratory Animals, published by the US National Institutes of Health (NIH publication, 8th Edition, 2011). Our research protocol was approved by the Fukushima Medical University Animal Research Committee. All animal experiments were performed in accordance with the guidelines of the Fukushima Medical University Animal Research Committee.

Rat MI model

Adult Sprague Dawley rats (10–13 weeks of age) were used in the experiments. The rats were anaesthetized by intra-peritoneal injection with medetomidine (0.1 mg/kg), midazoram (2.0 mg/kg) and butorphanol (2.5 mg/kg). Intubation was performed with a 20-gauge polyethylene catheter, and ventilated using a rodent ventilator (Shinano Manufacturing, Tokyo, Japan). MI was induced by ligation of the left anterior descending coronary artery (LAD) with 6-0 prolene sutures. Induction of MI was confirmed by the change of the anterior wall color to pale. Sham rats underwent the same operation but without a ligation of the coronary artery.

Protocol of immunohistochemistry

Both MI and sham rats were euthanized randomly 1 or 2 weeks after surgery (1 week MI group:

N=15, 2 weeks MI group: N=30, sham group: N=51). Bilateral SGs and the spinal cord collected from 4% paraformaldehyde perfused rats were cryoprotected and frozen in Tissue-Tek O.C.T for immunohistochemistry. Every 100 μm longitudinal sections (10 μm thickness) of the SGs and every 300 μm coronal sections (20 μm thickness) of the spinal cord were mounted on glass microscope slides. The mounted frozen sections were incubated with a solution of 0.5% Triton-X, 5% bovine serum albumin (Sigma-Aldrich, St. Louis, Missouri, U.S.A.) at room temperature for 30 minutes, and then incubated overnight at 4℃ in the primary antibody. SGs collected at 2 weeks after surgery were incubated in rabbit anti-tyrosine hydroxylase (TH) antibody (MAB 318-AF 555, 1:100, EMD Millipore, Billerica, Massachusetts, U.S.A.), mouse anti-growth-associated protein-43 (GAP43) antibody (MAB 347, 1:100, EMD Millipore), or mouse anti-choline acetyltransferase (ChAT) antibody (MAB 305, 1:100, EMD Millipore). Spinal cords at 2 weeks after surgery were incubated in goat anti-ChAT antibody (AB 144P, 1:100, EMD Millipore), and spinal cord at 1 week after surgery were incubated in a cocktail of goat anti-ChAT antibody (1:100) with rabbit anti-brain-derived neurotrophic factor (BDNF) antibody (AB1779SP, 1:100, EMD Millipore), rabbit anti-TrkB antibody (sc-12, 1:200, Santa Cruz Biotechnology, Santa Cruz, California, U.S.A.) or rabbit anti-phospho-extracellular signal-regulated kinase (pERK) (Thr202/Tyr204) antibody (#4370, 1:100, Cell Signaling Technology, Danvers, Massachusetts, U.S.A.). Following a series of rinses

with 1% PBS, the sections were incubated for one hour at room temperature in the appropriate secondary antibodies (Alexa 488 donkey anti-mouse, Alexa 488 donkey anti-rabbit, Alexa 594 donkey anti-goat, all at 1:1000, Abcam, Cambridge, U.K.), which were diluted in 1% PBS. As a control, tissues were processed with the omission of the primary antibodies. All images were captured using a BZ-X 700 microscope (Keyence, Osaka, Japan) and analyzed using BZ-X analyzer software (Keyence)

Analysis of immunohistochemistry

BZ-X analyzer software was used to determine the neuronal sizes and nerve densities of SGs and IMLs. The neuronal size was automatically measured by the color of the immunohistochemical stains and then calculated as the pixel area of the nerves. The positive nerve densities were expressed as the total area of all counted nerve fibers divided by the total area examined ($\mu m^2/mm^2$). The average fluorescence intensity within each cell was measured for the evaluation of the expression of BDNF and TrkB. Background intensity, defined as an area without cells, was measured, and the value was subtracted from the average fluorescence intensity of the cells. The percentage of pERK positive cells was carefully distinguished between negative and positive staining while comparing with the control images. A single blinded investigator randomly selected three fields for each section and averaged measured values on the selected fields.

mRNA analysis

Spinal cords at the Th2 level, collected from 0.9% saline perfused rats (1 week MI group: N=5, sham group: N=6), were immediately frozen in liquid nitrogen and stored in -80°C for further processing. Total RNA was extracted using TRIZOL reagent (Invitrogen, Waltham, Massachusetts, U.S.A.) according to the manufacturer's protocol. The concentrations in all RNA samples were determined spectrophotometrically. A cDNA was produced from total RNA using the ReverTra Ace qPCR RT Master Mix (ToYoBo Co., Ltd., Osaka, Japan) according to the manufacturer's instructions. The expression levels of candidate genes were measured by real-time quantitative RT-PCR (qRT-PCR) using SYBR Green PCR Master mix (Applied Biosystems, Waltham, Massachusetts, U.S.A.) and primers specific for rat on a CFX Connect (Bio-Rad Laboratories, Hercules, California, U.S.A.) according to the manufacturer's protocol. In each assay, β-actin was determined as internal control along with a target gene in each sample. The mRNA levels of each gene were calculated with the relative standard curve method and normalized against corresponding β-actin mRNA levels, and then expressed as relative change over control±SD. A single dissociation peak was detected in each reaction by a dissociation curve. Primers were designed based on the GenBank sequences. Table 1 shows the primer sequences and amplicon size of the selected genes.

Western blotting

The tissue samples of spinal cords at the Th2 level were obtained from the each group (1 week MI group: N=7, sham group: N=8). The total protein was extracted from the snap-frozen spinal cord using Cell Lysis Buffer (Cell Signaling Technology) with Protease Inhibitor Cocktail (BD Biosciences, San Jose, California, U.S.A.). The protein concentration of the sample was determined by protein assay (DC protein assay kit, Bio-Rad Laboratories, Hercules, California, U.S.A.). Equal amounts (20 μg) of the protein samples were subjected to electrophoresis onto sodium dodecyl sulfate polyacrylamide gel electrophoresis (SDS-PAGE, 10%) and transferred onto polyvinylidene difluoride membranes (ATTO Co., Tokyo, Japan). Membranes were blocked in Tris-buffered saline Tween 20 (TBST) containing 5% bovine serum albumin at room temperature for 60 minutes and were incubated overnight at 4℃ with the following primary antibodies: rabbit anti-pERK (Thr202/Tyr204) antibody (#9101, 1:1000, Cell Signaling Technology) and rabbit anti-ERK (Thr202/Tyr204) antibody (#9102, 1:1000, Cell Signaling Technology). Membranes were then washed in TBST, and incubated at room temperature for 60 minutes with the anti-rabbit horseradish peroxidase-linked secondary antibody (NA 934-100UL, 1:10000, GE healthcare, Chicago, Illinois, U.S.A.). The signals from the immunoreactive bands were visualized by an Amersham ECL system (Amersham Pharmacia Biotech UK Ltd., Buckinghamshire, U.K.) The relative intensities of the protein bands were quantified using NIH Image J, version (1.48) (Scion Image, NIH, Bethesda,

Maryland, U.S.A.).

Statistical analysis

All data are presented as mean±SD. Unpaired Student's t-test was used to compare the means for independent samples. On the other hands, paired Student's t-test was used to compare the means for paired samples. A value of $P<0.05$ was considered statistically significant. All analyses were performed using a statistical software package (SPSS ver. 23.0, IBM, Armonk, New York, U.S.A.).

Results

The neural remodeling in SG and IML after MI

In order to confirm neural remodeling in postganglionic sympathetic neurons after MI, the neuronal size was measured in SG. The size of TH-immunoreactive cell bodies in both right and left SGs was increased 2 weeks after MI compared to sham (Right 483.1±34.2 vs. 430.5±20.0 μm^2, $P<0.01$; Left 468.6±25.4 vs. 438.3±23.1 μm^2, $P<0.05$, respectively) (Fig.1, *A* and *B*). Next, the neuronal size in IML was examined after MI. ChAT-immunoreactive cell bodies, i.e. preganglionic sympathetic neurons, in both right and left IMLs were increased 2 weeks after MI compared to sham (Right 193.5±16.0 vs. 169.1±8.5 μm^2, $P<0.01$; Left 176.1±10.7 vs. 163.4±11.5 μm^2, $P<0.05$, respectively) (Fig. 1, *D* and *E*). The neuronal size in both SG and IML was not different between the right and left sides in the sham group, whereas the right side neuronal size in both SG and IML was larger than the left side in the MI group (Fig.1, *C* and *F*).

Fig. 2 shows the density of axons derived from preganglionic sympathetic neurons projecting to bilateral SGs. Consistent with the increased neuronal size in IML, the densities of ChAT-immunoreactive axons in the bilateral SGs were increased 2 weeks after MI compared to sham (Right 60587±21767 vs. 31380±17026 $\mu m^2/mm^2$, $P<0.05$; Left 55096±18265 vs. 30443±14537 $\mu m^2/mm^2$, $P<0.05$, respectively) (Fig. 2, *A* and *B*). The densities of ChAT-immunoreactive axons in

SG were not different between the right and left sides in both the sham and MI groups (Fig. 2, *C*). In addition, the densities of GAP43-immunoreactive nerve, a marker of nerve sprouting, in bilateral SGs were increased 2 weeks after MI compared to sham (Right 54750±20047 vs. 28668±12717 $\mu m^2/mm^2$, $P<0.05$; Left 53216±23186 vs. 29386±7033 $\mu m^2/mm^2$, $P<0.05$, respectively) (Fig. 2, *D* and *E*). The densities of GAP43-immunoreactive axons in SG were no different between the right and left sides in both the sham and MI groups (Fig. 2, *F*).

The mRNA expression of BDNF and TrkB in spinal cord

We next examined mRNA expression levels of the neurotrophic factors and their receptors in the spinal cord after MI. The mRNA expression of BDNF was increased 1 week after MI (1.8±0.9-fold change vs. sham, $P<0.01$) (Fig. 3*A*). The mRNA expression of TrkB, a receptor for BDNF, was also increased after MI (1.3±0.2-fold change vs. sham, $P<0.05$) (Fig. 3*B*). On the other hand, the mRNA expression of nerve growth factor (NGF) and its receptor TrkA was unchanged after MI (0.8±0.2-fold change vs. sham, *P*=N.S.; 1.1±0.2-fold change vs. sham, *P*=N.S.) (Fig. 3, *C* and *D*).

The fluorescence intensity of BDNF and TrkB in IML

Consistent with the increased expression of mRNA in the spinal cord, the fluorescence intensity for BDNF in bilateral IMLs was significantly higher in the MI group than in the sham group (Fig. 4, A, B, C and D). Similarly, the fluorescence intensity for TrkB in bilateral IMLs was also significantly

increased in MI compared to sham (Fig. 5, A, B, C and D). The fluorescence intensity for both BDNF and TrkB in IML was not different between the right and left sides in the MI group (Fig. 4*E and 5E*).

The activation of ERK in the spinal cord

We examined whether increased expressions of BDNF and TrkB resulted in activation of intracellular trophic signals in IML neurons. Western blot analysis showed that ERK was significantly activated after MI in the spinal cord at Th2 level (Fig. 6, *A* and *B*). Next, pERK-immunoreactive neurons were counted in IML 1 week after MI. The pERK was detected in both cytoplasm and nuclei, and the percentage of pERK-immunoreactive neurons in bilateral IMLs was significantly higher in the MI group than in the sham group (Fig. 6, *C, D, E* and *F*). The percentage of pERK-immunoreactive neurons in IML was not different between the right and left sides in the MI group (Fig. *6G*).

Discussion

The major findings of the present study are as follows: 1) neural remodeling was induced by MI as demonstrated by increased neuronal size in IML and GAP43 positive axonal density in SG, and 2) mRNA expression of BDNF and its receptor TrkB in the spinal cord was increased, and the fluorescence intensity of BDNF, TrkB in IML were higher after MI, and 3) phosphorylation activity of ERK and the percentage of pERK-immunoreactive neurons in IML were higher after MI. These results support our hypothesis that MI induces sympathetic nervous remodeling of IML via activation of the BDNF-TrkB axis.

Several studies have shown that neural remodeling of SG is induced after MI (2, 15, 20, 21, 26, 39). In contrast, little is known about the neural remodeling at the upper level of the sympathetic SNS for the heart. The present study demonstrated that neuronal size in IML and density of ChAT-, GAP43-positive axons in SG were increased after MI. These findings indicate that neuronal hypertrophy in IML and nerve sprouting from IML to SG, that is, neural remodeling of IML occurs after MI. To our knowledge, this is the first study to show that MI induces neuronal hypertrophy in IML.

Neurotrophic factors regulate differentiation, maintenance and survival of nerve cells through binding to Trk receptors (11, 33, 37). BDNF and its receptor TrkB are widely distributed in the

central nervous system (11, 22, 33, 37). In the present study, fluorescence intensity for TrkB protein in IML and TrkB mRNA in the spinal cord at the corresponding level were increased after MI, suggesting that TrkB expression is increased in IML after MI. Similarly, fluorescence intensity for BDNF protein, the most specific ligand for TrkB, in IML and BDNF mRNA in the spinal cord at the corresponding levels were increased after MI, but these findings do not necessarily prove that the expression of BDNF in IML is increased. It is possible that BDNF is produced and secreted by other types of cells, bound to TrkB and internalized into neurons in IML. A previous study by Conner et al. demonstrated that BDNF mRNA in the spinal cord is expressed only in the intermediate zone, where IML is located (7). Therefore, up-regulated BDNF in IML may be derived from preganglionic neurons inside IML by an autocrine mechanism and/or from glial cells surrounding the neurons inside or near IML by a paracrine mechanism.

The expression of BDNF is regulated by various transcriptional factors including cAMP response element binding protein (CREB), the nuclear factor of T cells, and the nuclear factor κB (16). TrkB expression was also regulated by CREB in neuronal cells (8, 13). A previous report showed that angiotensin II increased the expression of BDNF in rostral ventrolateral medulla（RVLM）via the phosphorylation of CREB (6). Another study by Iskra et al. showed that tumor necrosis factor-α (TNF-α) activated CREB via the p38 mitogen-activated protein kinase pathway, resulting in

increased expression of BDNF in trigeminal ganglion neurons (12). Thus, several lines of evidence clarified the mechanisms of upregulating BDNF and TrkB in central or peripheral nervous system, but the mechanisms in IML are still lacking. Plasma angiotensin II signals to the brain through circumventricular organs, which lack a tight blood brain barrier, in normal conditions (28). However, Biancardi et al. reported that increased angiotensin II can access to the paraventricular nucleus of the hypothalamus and RVLM parenchyma via disruption of blood brain barrier in hypertensive condition (4), suggesting that circulating angiotensin II can affect directly sympathoexcitatory centers in pathological state. Considering the following reports that angiotensin type 1 receptor expresses in IML neurons (1), and angiotensin II activated microglia resulting in increased proinflammatory cytokines including TNF-α and nuclear factor κB (32), it might be possible that pathologically increased levels of angiotensin II can access to IML neurons and/or microglia, leading to enhance the expression of BDNF and TrkB in IML.

Trk family members are receptor tyrosine kinases, activated by the binding of neurotrophic factors, which are autophosphorylates themselves, and thereby triggers various trophic signals including Ras-ERK axis, Src, phosphoinositide 3-kinase-Akt axis, and phospholipase C-γ. These signal events are involved in sprouting, migration and hypertrophy of neurons. We showed that ERK is activated in preganglionic neurons in IML after MI. As mentioned earlier, BDNF and TrkB expressions were

increased after MI. In contrast to BDNF and TrkB expression in IML, we could not detect a significant increase in NGF and its receptor TrkA after MI. NGF and its receptor TrkA are mainly distributed in the peripheral nervous system and restricted to defined areas of the central nervous system. Michael et al. reported that there were no TrkA-immunoreactive neurons in IML (19). Other studies have showed that preganglionic neurons did not respond to NGF (23, 31), probably because TrkA was not expressed in preganglionic neurons. Thus, the NGF-TrkA axis may exclusively be involved in neural remodeling of SG after MI, which belongs to the peripheral nervous system (15, 20, 21, 39). In addition, we could not detect TrkC in IML (unpublished data). Therefore, it is likely that activation of ERK after MI is due to increased expression of the BDNF-TrkB axis in IML, which leads to neuronal hypertrophy of IML and sprouting into SG.

In our study, the right side neuronal size in SG after MI was larger than the left side. Several studies have shown that the right side SG innervates predominantly the anterior aspect of the left ventricle (LV), whereas the left side SG innervates predominantly the posterior aspect of the LV (27, 36, 38). In addition, NGF released from the infarct site and retrogradely transported to SG causes neural remodeling of SG (15, 20, 21, 39). Because we created MI in the anterior aspect of LV, the amount of NGF in the right side might be larger than in the left side, resulting in right side dominant neuronal hypertrophy of SG. Right side dominant neuronal hypertrophy was also observed in IML. It

has been shown that TNF-α was released from mainly the infarct site after MI (34). Lin et al. reported expressions of BDNF and TrkB in the spinal dorsal root ganglion (DRG) was upregulated by TNF-α released from the inflammatory area and retrogradely transported to the DRG (14). Because cardiac afferent nerves are also distributed in IML, TNF-α released from the infarct site may retrogradely transported to IML, involving in increased expressions of BDNF and TrkB. On the other hands, axonal density of IML, BDNF, TrkB protein expressions and ERK activity in IML were not different between the right and left sides. These results were conflicting with the above mechanisms. In this study, these experiments were performed by the immunohistochemistry. There is a possibility that the capability of the immunohistochemistry was not enough to detect subtle differences between the right and left sides.

Until recently, sympathetic nervous remodeling in MI has been well documented in the context of sympathetic efferent regeneration to repair disrupted sympathetic nerve innervation between infarct myocardium and SG. In the present study, we first demonstrated the evidence of neural remodeling in both IML and SG, suggesting a novel concept that neural remodeling may involve whole SNS. It seems reasonable to hypothesize that sympathetic neuronal hypertrophy is a compensatory response to overcome acute heart failure by means of sustained activation of sympathetic tone. However, sustained over-activation of the SNS causes the worsening of heart failure in the chronic phase and

development of fatal ventricular tachyarrhythmia (16, 34). Thus, further studies are needed to elucidate the pathophysiological mechanisms of neural remodeling throughout the SNS, which may lead to provide a novel approach for suppressing abnormal sympathetic excitement after MI.

Conclusion

We demonstrated that neuronal remodeling in IML probably via activation of the BDNF-TrkB axis after MI. The morphological remodeling throughout the SNS may be involved in its sustained activation after MI.

Disclosures

None.

Acknowledgments

We thank Drs. Masayoshi Oikawa, Ryoji Fukabori, Shigeki Kato, Naoki Tomikawa, Takafumi Ishida, Kazuto Kobayashi and Yasuchika Takeishi for their valuable comments on the present study, and Ms. Tomiko Miura for her excellent technical assistance.

References

1. **Ahmad Z, Milligan CJ, Paton JF, Deuchars J.** Angiotensin type 1 receptor immunoreactivity in the thoracic spinal cord. *Brain Res* 985: 21-31, 2003.

2. **Ajijola OA, Yagishita D, Reddy NK, Yamakawa K, Vaseghi M, Downs AM, Hoover DB, Ardell JL, Shivkumar S**. Remodeling of stellate ganglion neurons following spatially targeted myocardial infarction: neuropeptide and morphologic changes. *Heart Rhythm* 12: 1027-1035, 2015.

3. **Billman GE.** A comprehensive review and analysis of 25 years of data from an in vivo canine model of sudden cardiac death: implications for future anti-arrhythmic drug development. *Pharmacol Ther* 111: 808-835, 2006.

4. **Blancardi VC, Son SJ, Ahmadi S, Filosa JA, Stem JE.** Circulating angiotensin II gains access to the hypothalamus and brain stem during hypertension via breakdown of the blood-brain barrier. *Hypertension* 63: 572-579, 2014.

5. **Causing CG, Gloster A, Aloyz R, Bamji SX, Chang E, Fawcett J, Kuchel G, Miller FD.** Synaptic innervation density is regulated by neuron-derived BDNF. *Neuron* 18: 257-267, 1997.

6. **Chan SH, Wu CW, Chang AY, Hsu KS, Chan. JY.** Transcriptional upregulation of brain-derived neurotrophic factor in rostral ventrolateral medulla by angiotensin II significance in superoxide homeostasis and neural regulation of arterial pressure. *Circ Res* 107: 1127-1139, 2010.

7. **Conner JM, Lauterborn JC, Yan Q, Gall CM, Varon S.** Distribution of brain-derived neurotrophic factor (BDNF) protein and mRNA in the normal adult rat CNS: evidence for anterograde axonal transport. *J Neurosci* 1: 2295-2313, 1997.

8. **Deogracias R, Espliguero G, Iglesias T, Pena AR.** Expression of the neurotrophin receptor trkB is regulated by the cAMP/CREB pathway in neurons. *Mol Cell Neurosci* 26: 470-480, 2004.

9. **Du XJ, Dart AM**. Role of sympathoadrenergic mechanisms in arrhythmogenesis. *Cardiovasc Res* 43: 832-834, 1999.

10. **Han S, Kobayashi K, Joung B, Piccirillo G, Maruyama M, Vinters HV, March K, Lin SF, Shen C, Fishbein MC, Chen PS, Chen LS**. Electroanatomic remodeling of the left stellate ganglion after myocardial infarction. *J Am Coll Cardiol* 59: 954-961, 2012.

11. **Huang EJ, Reichardt LF.** Neurotrophins: Roles in neuronal development and function. *Annu Rev Neurosci* 24: 677-736, 2001.

12. **Iskra EB, Schmaedick AV, Balkowiec A, Sorkin LS.** Tumor necrosis factor-α increases BDNF expression in trigeminal ganglion neurons in an activity-dependent manner. *Neuroscience* 180: 322-333, 2011.

13. **Lei L, Parada LF.** Transcriptional regulation of Trk family neurotrophin receptors. *Cell Mol Life Sci* 64: 522-532, 2007.

14. **Lin YT, Ro LS, Wang HL, Chen JC.** Up-regulation of dorsal root ganglia BDNF and trkB receptor in inflammatory pain: an in vivo and in vitro study. *J Neuroinflammation* 8: 126, 2011.

15. **Li Z, Wang M, Zhang Y, Zheng S, Wang X, Hou Y**. The effect of the left stellate ganglion on sympathetic neural remodeling of the left atrium in rats following myocardial infarction. *Pace* 38: 107-114, 2015.

16. **Lymperopoulos A, Rengo G, Koch WJ.** The adrenergic nervous system in heart failure: pathophysiology and therapy. *Circ Res* 113: 759-763, 2013.

17. **Lyons MR, West AE.** Mechanisms of specificity in neuronal activity-regulated gene transcription. *Prog Neurobiol* 94: 259–295, 2011.

18. **McCartney AM, Abejuela L, Isaacson LG.** Characterization of trkB immunoreactive cells in the intermediolateral cell column of the rat spinal cord. *Neurosci Lett* 440: 103-108, 2008.

19. **Michael GJ, Kaya E, Averill S, Rattray M, Clary DO, Priestley JV.** TrkA immunoreactive neurons in the rat spinal cord. *J Comp Neurol* 385: 441-455, 1997.

20. **Nguyen BL, Li H, Fishbein MC, Lin SF, Gaudio C, Chen PS, Chen LS.** Acute myocardial infarction induces bilateral stellate ganglia neural remodeling in rabbits. *Cardiovasc Pathol* 21: 143-148, 2012.

21. **Oh YS, Jong AY, Kim DT, Li H, Wang C, Zemljic–Harpf A, Ross RS, Fishbein MC, Chen PS, Chen LS.** Spatial distribution of nerve sprouting after myocardial infarction in mice. *Heart Rhythm* 3: 728-736, 2006.

22. **Okada S, Yokoyama M, Toko H, Tateno K, Moriya J, Shimizu I, Nojima A, Ito T, Yoshida Y, Kobayashi Y, Katagiri H, Minamino T, Komuro I.** Brain-derived neurotrophic factor protects against cardiac dysfunction after myocardial infarction via central nervous system-mediated pathway. *Arterioscler Thromb Vasc Biol* 32: 1902-1909, 2012.

23. **Oppenheim R.W, Maderdrut, JL, Wells DJ.** Cell death of motoneurons in the chick embryo spinal cord. VI. Reduction of naturally occurring cell death in the thoracolumbar column of Terni by nerve growth factor. *J Comp Neurol* 210: 174-189, 1982.

24. **Pardini BJ, Lund DD, Schmid PG.** Organization of the sympathetic postganglionic innervation of the rat heart. *J Auton Nerv Syst* 28: 193-201, 1989.

25. **Pardini BJ, Lund DD, Schmid PG.** Innervation patterns of the middle cervical-stellate ganglion complex in the rat. *Neurosci Lett* 117: 300-306, 1990.

26. **Rajendran PS, Nakamura K, Ajijola OA, Vaseghi M, Armour JA, Ardell JL, Shivkumar K.** Myocardial infarction induces structural and functional remodeling of the intrinsic cardiac nervous system. *J Physiol* 594: 321-341, 2016.

27. **Ramirez RJ, Ajijola OA, Zhou W, Holmstrom B, Luning H, Laks MM, Shivkumar K, Mahajan A.** A new electrocardiographic marker for sympathetic nerve stimulation: modulation of repolarization by stimulation of stellate ganglia. *J Electrocardiol* 44: 694–699, 2011.

28. **Roig E, Perez-Villa F, Morales M, Jimenez W, Orus J, Heras M, Sanz G.** Clinical implications of increased plasma angiotensin II despite ACE inhibitor therapy in patients with congestive heart failure. *Eur Heart J* 21: 53-57, 2000.

29. **Rubart M, Zipes DP.** Mechanisms of sudden cardiac death. *J Clin Invest* 115: 2305-2315, 2005.

30. **Schober A, Wolf N, Kahane N, Kalcheim C, Krieglstein K, Unsicker K.** Expression of neurotrophin receptors trkB and trkC and their ligands in rat adrenal gland and the intermediolateral column of the spinal cord. *Cell Tissue Res* 296: 271-279, 1999.

31. **Schwab ME, Thoenen H.** Selective trans-synaptic migration of tetanus toxin after retrograde axonal transport in peripheral sympathetic nerves: A comparison with nerve growth factor. *Brain Res* 122: 459-474, 1977.

32. **Shi P, Diez-Fieier C, Jun JY, Qi Y, Katovich MJ, Li Q, Sriamula S, Francis J, Sumners C, Raizada MK.** Brain microglial cytokines in neurogenic hypertension. *Hypertension* 56: 297-303, 2010.

33. **Skaper SD.** The neurotrophin family of neurotrophic factors: an overview. *Methods Mol Biol* 846: 1-12, 2012.

34. **Tian M, Yuan YC, Li JY, Gionfriddo MR, Huang RC.** Tumor necrosis factor-α and its role as a mediator in myocardial infarction: A brief review. *Chronic Dis Transl Med* 1: 18-26, 2015.

35. **Triposkiadis F, Karayannis G, Giamouzis G, Skoularigis J, Louridas G, Butler J.** The sympathetic nervous system in heart failure physiology, pathophysiology, and clinical implications. *J Am Coll Cardiol* 54: 1747-1762, 2009.

36. **Ueda H, Yanai Y, Murao S, Harumi K, Mashima S, Kuroiwa A, Sugimoto T, Shimomura D.** Electrocardiographic and vectorcardio- graphic changes produced by electrical stimulation of the cardiac nerves. *Jpn Heart J* 28: 359 –372, 1964.

37. **Wiesmann C, de Vos AM.** Nerve growth factor: structure and function. *Cell Mol Life Sci* 58: 748-759, 2001.

38. **Yanowitz F, Preston JB, Abildskov JA.** Functional distribution of right and left stellate innervation to the ventricles. Production of neurogenic electrocardiographic changes by unilateral alteration of sympathetic tone. *Circ Res* 18: 416 –428, 1966.

39. **Zhou S, Chen LS, Miyauchi Y, Miyauchi M, Kar S, Kangavari S, Fishbein MC, Sharifi B, Chen PS.** Mechanisms of cardiac nerve sprouting after myocardial infarction in dogs. *Circ Res* 95: 76-83, 2004.

40. **Zhou S, Jung B-C, Tan AY, Trang VQ, Gholmieh G, Han SW, Lin SF, Fishbein MC, Chen PS, Chen LS.** Spontaneous stellate ganglion nerve activity and ventricular arrhythmia in a canine model of sudden death. *Heart Rhythm* 5: 131-139, 2008.

Table.1 Primer sequence and amplicon size of genes evaluated by qRT-PCR

Gene Name	Primer sequence	Amplicon size, bp
β-actin	F: 5'-GGAGATTACTGCCCTGGCTCCTA-3' R: 5'-GACTCATCGTACTCCTGCTTGCTG-3'	150
BDNF	F: 5'-CAGCGCGAATGTGTTAGTGTTA-3' R: 5'-CAGTGGACAGCCACTTTGTTTCA-3'	112
TrkB	F: 5'-GTGGATTCCGGCTTAAAGTTTGTG-3' R: 5'-CAAGTCAAGGTGGCGGAAATG-3'	126
NGF	F: 5'-TGCCAAGGACGCAGCTTTC-3' R: 5'-TGAAGTTTAGTCCAGTGGGCTTCAG-3'	171
TrkA	F: 5'-TGCTCAACAAATGTGGACAGAGG-3' R: 5'-TGTCATGAAGTGTAGGGACATGG-3'	98

BDNF, brain-derived neurotrophic factor; TrkB, tropomyosin receptor kinase B; NGF, nerve growth factor; TrkA, tropomyosin receptor kinase A.

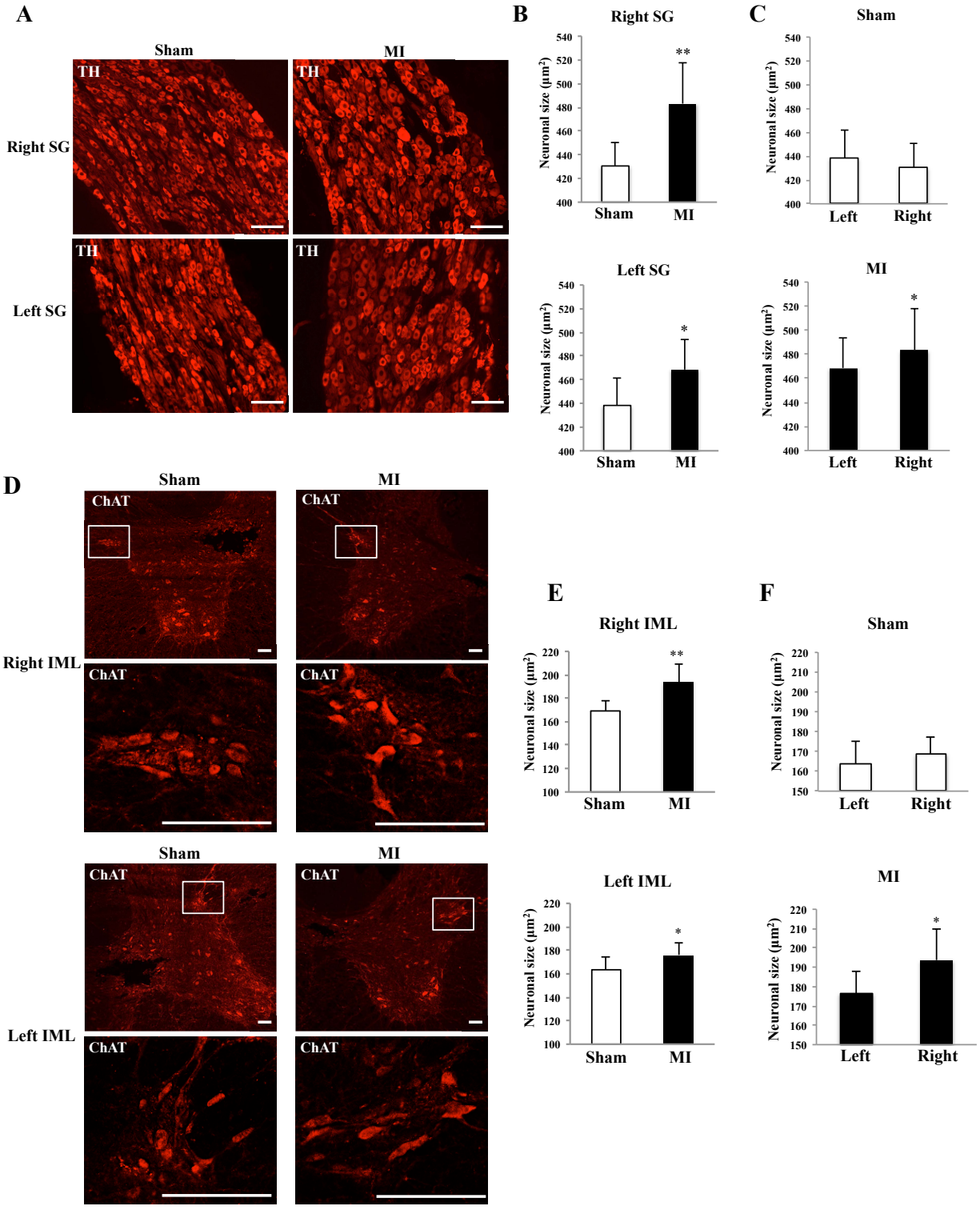

Fig. 1. Neuronal cell body hypertrophy in SG and IML 2 weeks after MI.

A: Images of TH-immunofluorescence staining sections of bilateral SGs in sham and MI rats (scale bar: 100 μm). *B*: Comparison of TH-immunoreactive neuronal size in bilateral SGs between sham and MI rats. *C*: Comparison of TH-immunoreactive neuronal size between right and left SGs in sham and MI rats. *D*: Images of ChAT-immunofluorescence staining sections of bilateral IMLs of sham and MI rats (scale bar: 100 μm). *E*: Comparison of ChAT-immunoreactive neuronal size in bilateral IMLs between sham and MI rats. *F*: Comparison of ChAT-immunoreactive neuronal size between right and left IMLs in sham and MI rats. Values are means±SD. **P* < 0.05, ***P* < 0.01 vs. sham. N=10 or 11 in each group.

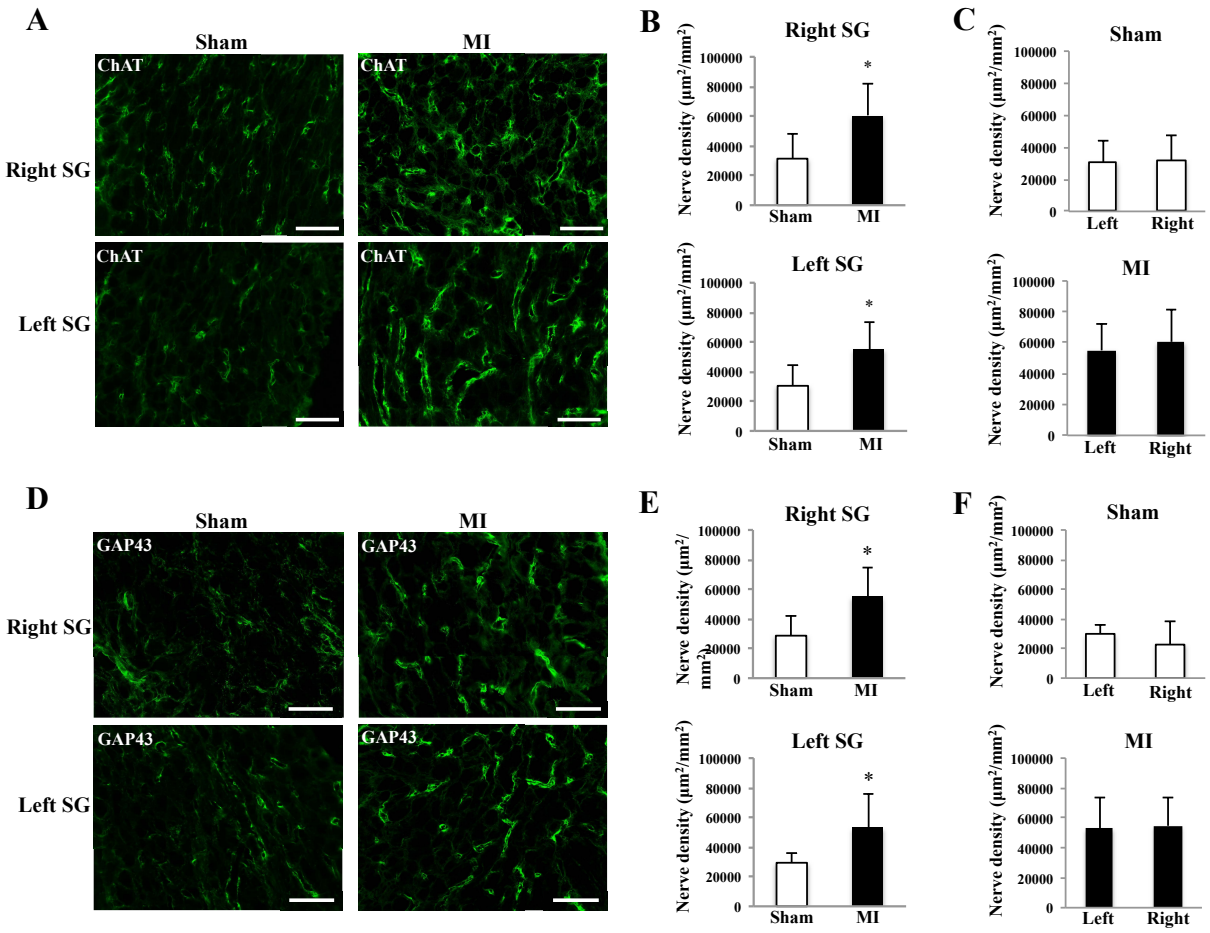

Fig. 2. The density of axons derived from preganglionic sympathetic neuron projecting to SG 2 weeks after MI.

A: Images of ChAT-immunofluorescence staining sections of bilateral SGs in sham and MI rats (scale bar: 100 μm). *B*: Comparison of ChAT-immunoreactive nerve density in bilateral SGs between sham and MI rats. *C*: Comparison of ChAT-immunoreactive nerve density between right and left SGs in sham and MI rats. *D*: Images of GAP43-immunofluorescence staining sections of bilateral SGs in sham and MI rats (scale bar: 100 μm). *E*: Comparison of GAP43-immunoreactive nerve density in bilateral SGs between sham and MI rats. *F*: Comparison of GAP43-immunoreactive nerve density between right and left SGs in sham and MI rats. **P* < 0.05 vs. sham. N=10 or 11 in each group.

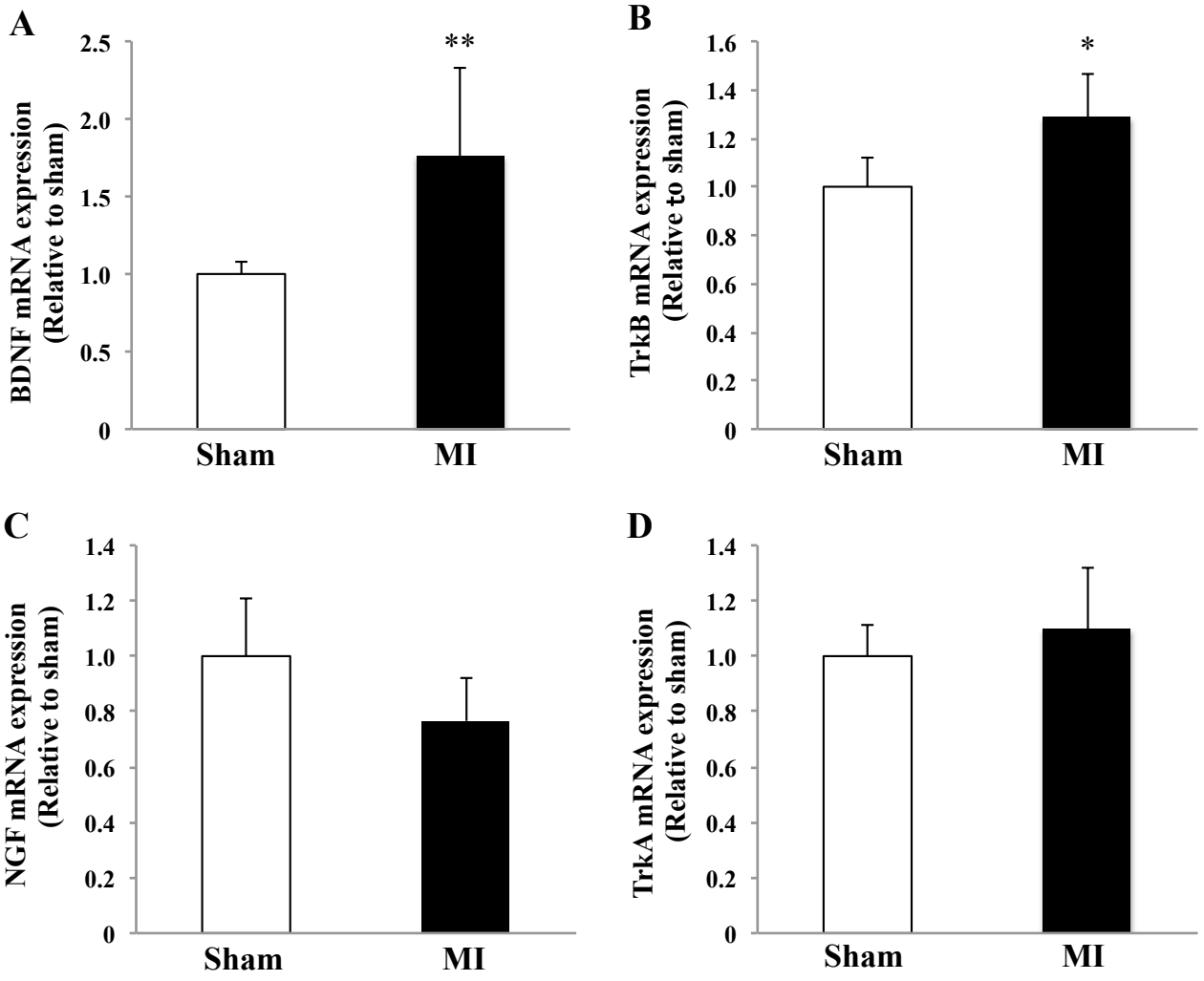

Fig. 3. Gene expressions of BDNF (*A*), TrkB (*B*), NGF (*C*), and TrkA (*D*) in spinal cord 1 week after MI. **P* < 0.05, ***P* < 0.01 vs. sham. N=5 or 6 in each group.

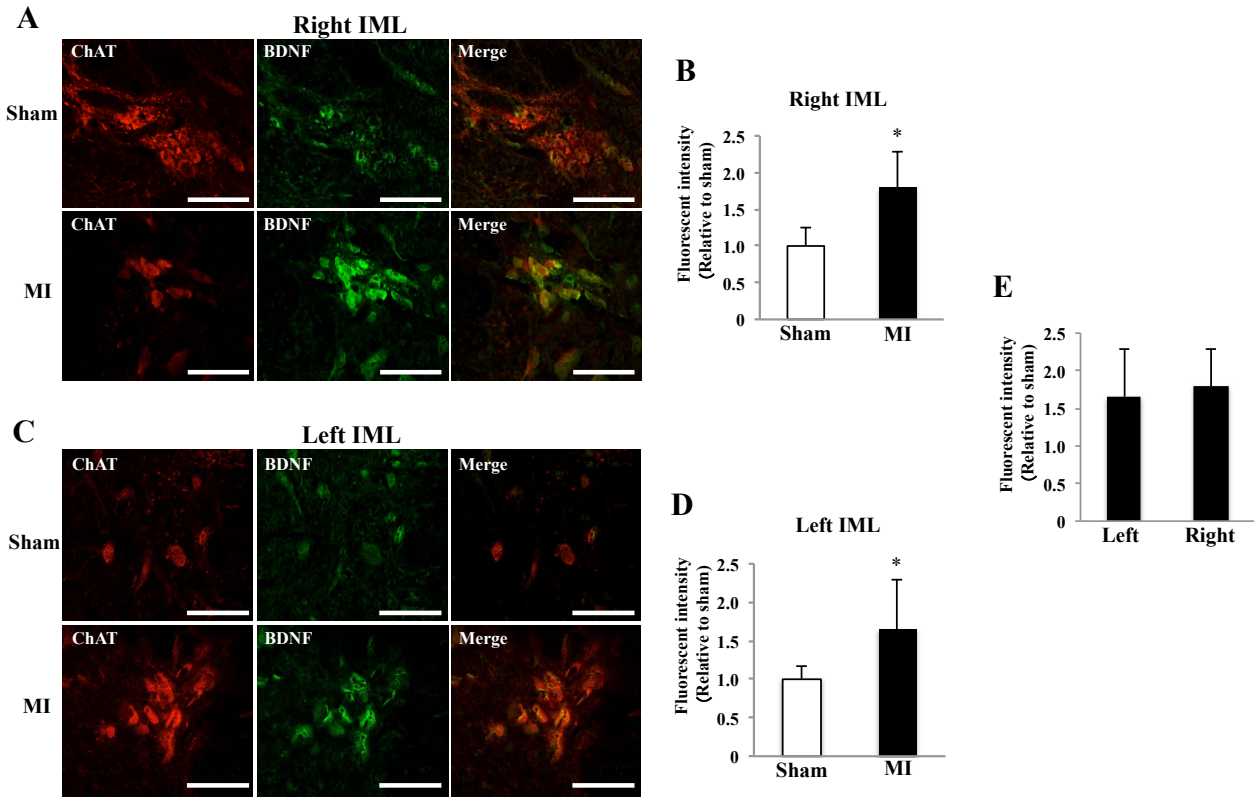

Fig. 4. Fluorescence intensity of BDNF in IML 1 week after MI

A: Images of double immunofluorescence staining (ChAT and BDNF) sections of right IML of sham and MI rats (scale bar: 50 μm). *B*: Comparison of immunofluorescence intensity of BDNF in right IML between sham and MI rats. *C*: Images of double immunofluorescence staining (ChAT and BDNF) sections of left IML of sham and MI rats (scale bar: 50 μm). *D*: Comparison of immunofluorescence intensity of BDNF in left IML between sham and MI rats. *E*: Comparison of immunofluorescence intensity of BDNF between right and left IMLs in MI rats. **P* < 0.05 vs. control. N=5 or 6 in each group.

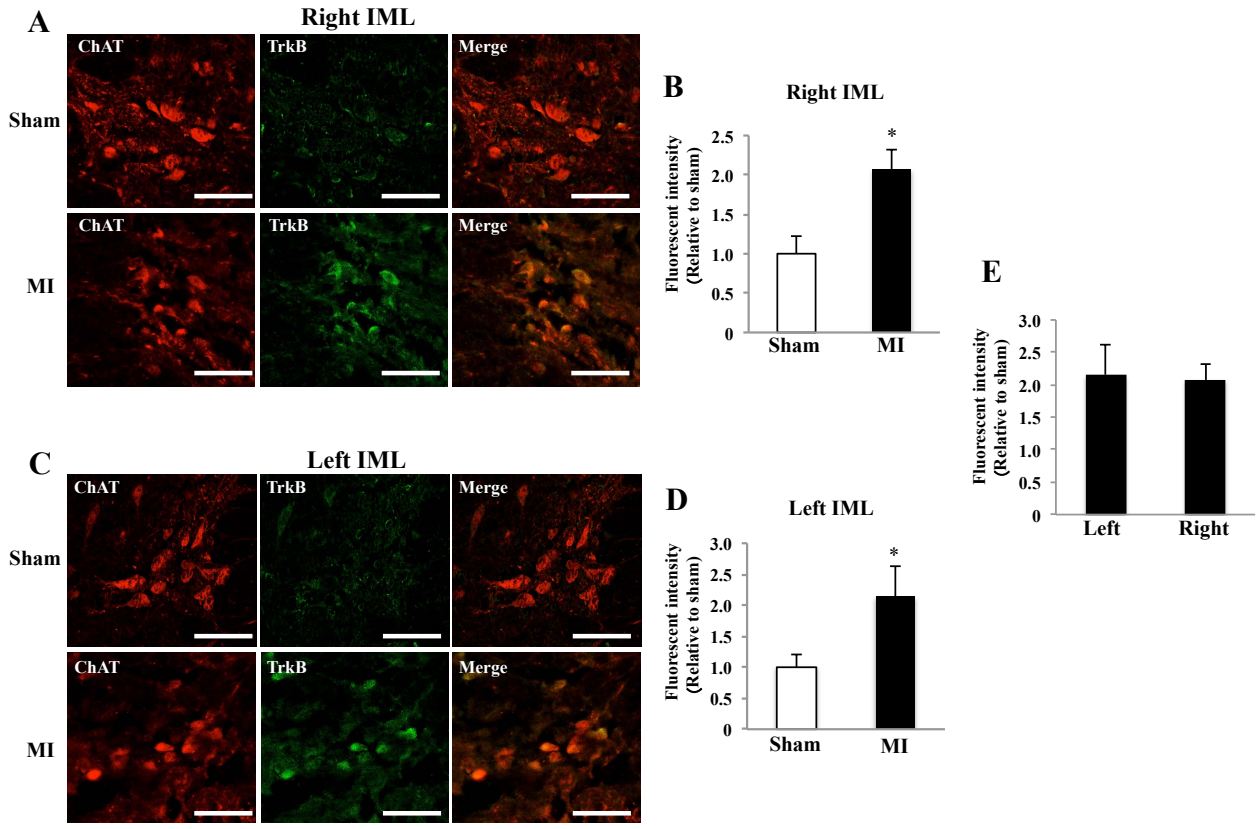

Fig. 5. Fluorescence intensity of TrkB in IML 1 week after MI

A: Images of double immunofluorescence staining (ChAT and TrkB) sections of right IML of sham and MI rats (scale bar: 50 μm). *B*: Comparison of immunofluorescence intensity of TrkB in right IML between sham and MI rats. *C*: Images of double immunofluorescence staining (ChAT and TrkB) sections of left IML of sham and MI rats (scale bar: 50 μm). *D*: Comparison of immunofluorescence intensity of TrkB in left IML between sham and MI rats. *E*: Comparison of immunofluorescence intensity of TrkB between right and left IMLs in MI rats. **P* < 0.05 vs. control. N=5 or 6 in each group.

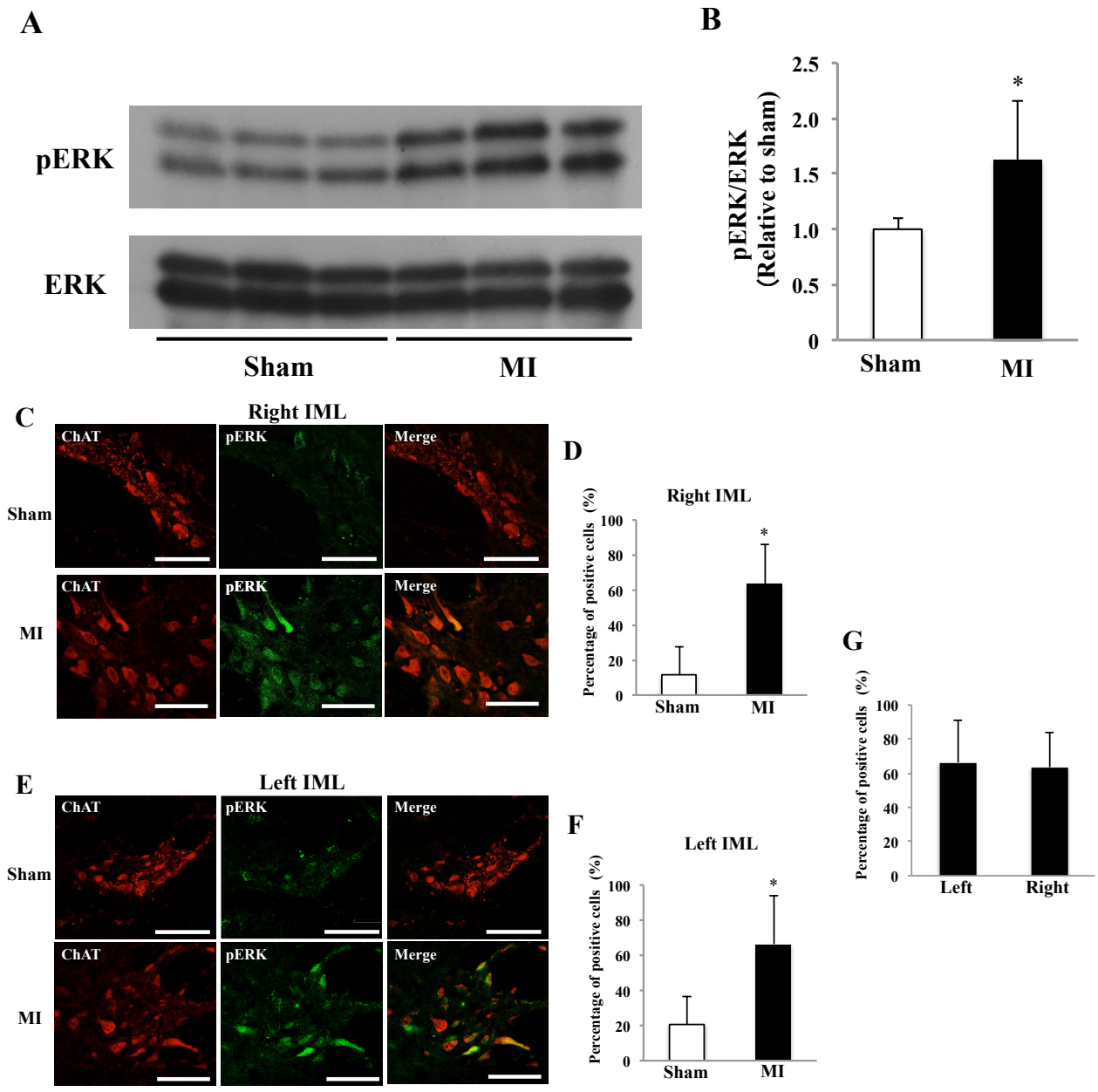

Fig. 6. The activation of ERK in the spinal cord 1 week after MI

A: Representative Western blot of pERK and total ERK in the spinal cord of sham and MI rats. *B:* Comparison of pERK/ERK ratio in the spinal cord between sham and MI rats. **P* < 0.05 vs. sham. N=7 or 8 in each group. *C:* Images of double immunofluorescence staining (ChAT and pERK) sections of right IML of sham and MI rats (scale bar: 50μm). *D*: Comparison of the percentage of pERK positive neurons in right IML between sham and MI rats. *E*: Images of double immunofluorescence staining (ChAT and pERK) sections of left IML of sham and MI rats (scale bar: 50μm). *F*: Comparison of the percentage of pERK positive neurons in left IML between sham and MI rats. *G*: Comparison of the percentage of pERK positive neurons between right and left IMLs in MI rats. **P* < 0.05 vs. sham. N=5 or 6 in each group.